

## Supplemental Information

# Shaken, not stirred: Collapsing a peptoid monolayer to produce free-floating, stable nanosheets

Babak Sani, Romas Kudirka, Andrew Cho, Neeraja Venkateswaran,  
Gloria K. Olivier, Alexander M. Olson, Helen Tran,  
R. Marika Harada, Li Tan and Ronald N. Zuckermann\*

## Contents

<b>1</b>	<b>Agitation mechanics and nanosheet production</b>	<b>2</b>
<b>2</b>	<b>Movies of free-floating nanosheets in solution</b>	<b>4</b>
<b>3</b>	<b>Surface area of liquid in a cuvette during rotation</b>	<b>5</b>
3.1	Analysis . . . . .	5
3.2	Modeling . . . . .	10
<b>4</b>	<b>AFM analysis of nanosheet and monolayer heights</b>	<b>11</b>
<b>5</b>	<b>Powder X-ray diffraction analysis</b>	<b>13</b>
<b>6</b>	<b>Sheet counting image analysis software</b>	<b>14</b>
<b>7</b>	<b>Peptoid concentration effects</b>	<b>16</b>
<b>8</b>	<b>Zwittergent 3-12 inhibition of nanosheet production</b>	<b>17</b>
<b>9</b>	<b>Surface pressure reduction after multiple compressions</b>	<b>18</b>
<b>10</b>	<b>Nanosheet formation by interfacial contact</b>	<b>19</b>
<b>11</b>	<b>Peptoid synthesis</b>	<b>21</b>
<b>12</b>	<b>Solvatochromic dye conjugate structure</b>	<b>22</b>
<b>13</b>	<b>The vial rocking device</b>	<b>23</b>

---

\*rnzuckermann@lbl.gov

# 1 Agitation mechanics and nanosheet production

We qualitatively assessed nanosheet production as a function of agitation methods by applying a different method to each of five vials of nanosheet forming solution, and then analyzing the subphase by interference contrast optical microscopy for the presence of nanosheets. The nanosheet forming solutions consisted of 10  $\mu\text{M}$  (Nae-Npe)<sub>18</sub> and (Nce-Npe)<sub>18</sub> peptoids that were combined in a 10mM AMPD buffer, 100mM NaCl pH 9 solution, and gently mixed by pipette aspiration. The solutions were placed in five standard cylindrical vials (glass, 3.5cm height, 0.5cm diameter) within 5 minutes, and sampled 24 hrs later within 15 min. In the intervening 22 hours each vial was subjected to a different agitation method (see table 1).

**Table 1:** Agitation methods seen in Fig. S1.

Agitation Method	Experimental Details	Sheets
Stirred	PTFE stir-rod rotated at 50 RPM for 22 hours	No
Stationary	On table-top for 22 hrs	No
Rotated (w/o air)	22 hrs of 0.6 RPM rotation of a completely filled vial (along with a glass pipette tip)	No
Shaken	500 $\mu\text{L}$ volume shaken 10x by hand, after sitting for 22 hours	Yes
Rotated (with air)	22 hrs of 0.6 RPM rotation of a partially filled (500 $\mu\text{L}$ ) vial	Yes

We ascertained sheet production by aliquoting 2  $\mu\text{L}$  of the solution in each vial onto porous 1% agarose gels. Agarose gel was made by mixing 1% by weight powdered agarose (Sigma) into pure Milli-Q water and microwaving for  $\approx 30$  s to homogenize and dissolve the mixture. The agarose solution was poured into large petri dishes and allowed to cool and set. The peptoid solutions from the vials were placed onto cut  $\approx 1$  cm<sup>2</sup> squares of agarose gel, and allowed to sit for  $\approx 3$ min so that the solutes filter beneath the agarose surface, leaving macroscopic material (pore size  $\approx 500\text{nm}$ [1]) on the gel surface. The filtered material was readily imaged by differential interference contrast optical microscopy (Leica DM4000) without fluorescence labeling (see Fig. S1).

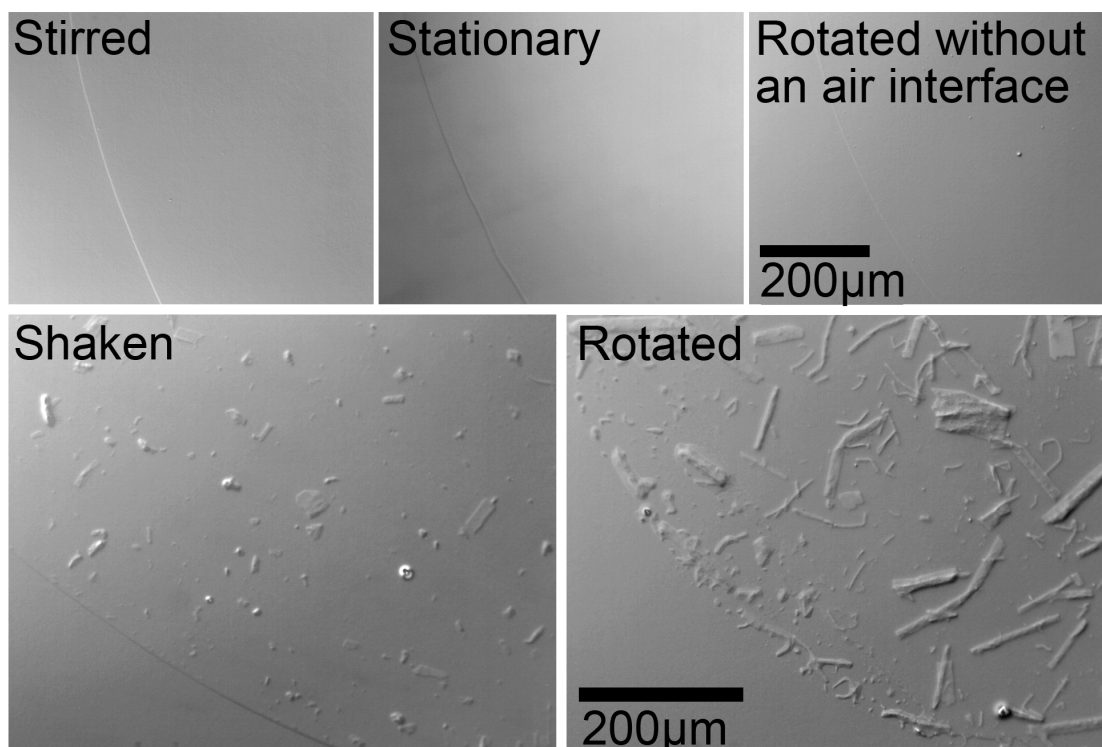


**Figure S1:** Optical images of the edge of 2  $\mu\text{L}$  droplets of peptoid solutions agitated in five different ways (labeled, see also table 1) after filtering through 1 % agarose gel.

## 2 Movies of free-floating nanosheets in solution

Two movies of free-floating nanosheets in solution are included in the supplemental information, illustrating the result of shaking and surface-compression agitation methods. Both movies are sped up approximately 18-fold, consist of a scanning  $1391\ \mu\text{m} \times 1059\ \mu\text{m}$  field of view and are of a nanosheet forming solutions of  $10\ \mu\text{M}$  (Nae-Npe)<sub>18</sub> and (Nce-Npe)<sub>18</sub> peptoids combined in a 10mM AMPD buffer, 100mM NaCl pH 9 solution, gently mixed by pipette aspiration prior to the respective agitation methods. The solutions were stained in  $1\ \mu\text{M}$  Nile Red and diluted 4X prior to deposition in an 0.12 mm deep well on a glass microscope slide, for imaging. The slide was centrifuged for 20 minutes at 350 rpm to place the sheets in one plane for imaging.

The sheets in the movie *nanosheets\_by\_shaking.mov* were manually shaken for 30s then left stationary for 1 minute. This cycle was repeated 5 times in total. The sheets in the movie *nanosheets\_by\_vial\_rotation.mov* were compressed by periodic rocking back and forth of their enclosing vial. The vial (glass, 3.5 x 1 cm) was rocked 348 times with the homemade instrument described below. Between compressions the vial was left in a horizontal position (85 degrees from vertical) for 450s.

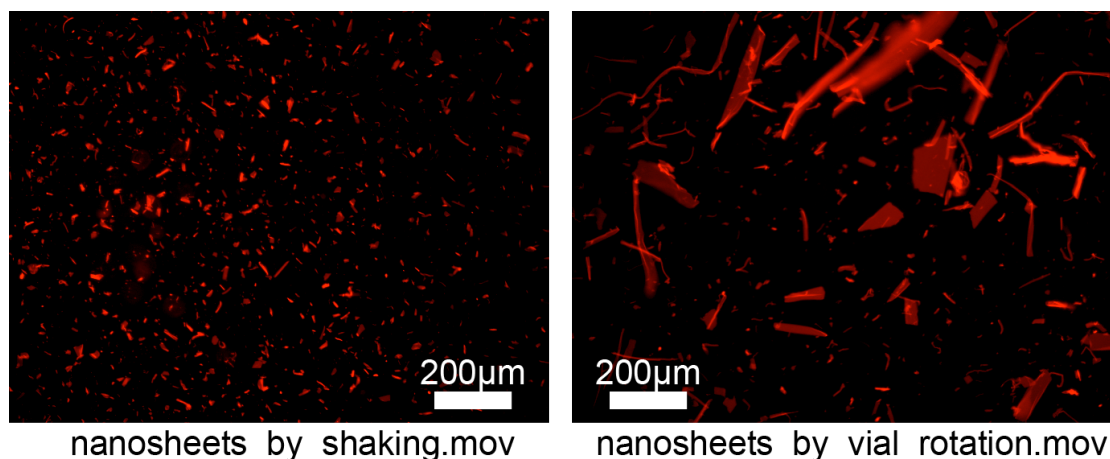


**Figure S2:** A frame from each of the included movies *nanosheets\_by\_shaking.mov* (left) and *nanosheets\_by\_vial\_rotation.mov* (right). Both images have a  $1391\ \mu\text{m} \times 1059\ \mu\text{m}$  field of view.

### 3 Surface area of liquid in a cuvette during rotation

#### 3.1 Analysis

Here we determine the exposed surface area of a given volume of liquid 'V' in a square-bottom cuvette of dimensions 'a' × 'a' × 'b', with its long axis 'b' rotated at an angle 'θ' from horizontal (with respect to uniform gravity). We consider the case where the vial is ≤ half full. We perform the analysis piece-wise in three regions defined by the contact points between the liquid and the walls of the cuvette, at angles defined below. The analysis occurs in the reference frame of the cuvette, where rotation with respect to gravity manifests as the liquid filling different portions of the cuvette, ignoring meniscus effects.

##### 3.1.1 Part 1

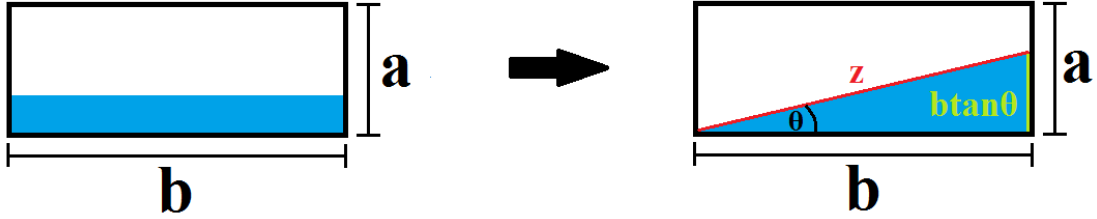


**Figure S3:** Definition of part 1 of the cuvette rotation

In part 1, the cuvette rotates from an initial angle of  $\theta_1 = 0$  to the angle at which the the surface of the liquid comes in contact with the bottom left corner of the cuvette in Fig. S3. This rotation angle corresponds to a right triangle of interior angle  $\theta_2$ , base of length 'b', and height  $b \tan(\theta_2)$ . Since the volume of the solution is the product of the depth and the area of the triangle, we determine the angle of rotation that satisfies this condition as follows:

$$V = (a) \left( \frac{1}{2} \right) (b) (b \tan \theta_2) \quad (1)$$

$$V = \frac{ab^2 \tan \theta_2}{2} \quad (2)$$

$$\frac{2V}{ab^2} = \tan \theta_2 \quad (3)$$

$$\theta_2 = \arctan \frac{2V}{ab^2} \quad (4)$$

Therefore, in part 1 the cuvette rotates from  $\theta = 0$  to  $\theta = \arctan \left( \frac{2V}{ab^2} \right)$ . Within this range of angles, we determine the value of the cross-sectional surface length 'z' (see Fig. S4) using the Pythagorean theorem.

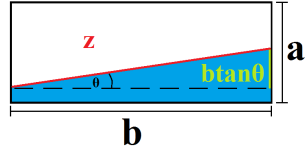


**Figure S4:** Cross-sectional view at an angle of rotation  $\theta$  in part 1.

$$z = \sqrt{b^2 + b^2 \tan^2 \theta} \quad (5)$$

$$= b\sqrt{1 + \tan^2 \theta} \quad (6)$$

$$= b\sqrt{\sec^2 \theta} \quad (7)$$

$$= b \sec \theta \quad (8)$$

As the surface area (SA) of the solution is equal to the product of the cuvette depth 'a' and the cross-sectional surface-length 'z', we represent the SA of part 1 as the following function of  $\theta$ :

$$SA_1(\theta) = ab \sec \theta, \quad \theta : \left[0, \arctan \frac{2V}{ab^2}\right) \quad (9)$$

### 3.1.2 Part 2

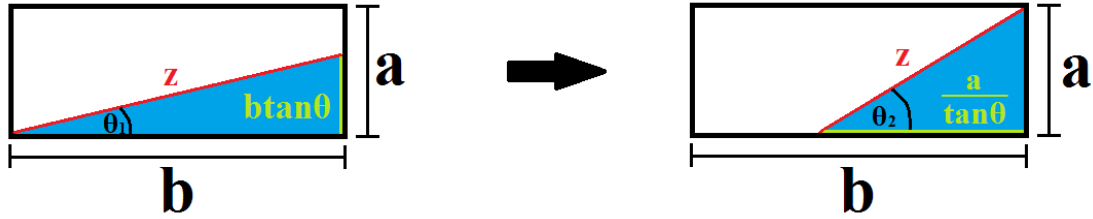


**Figure S5:** Definition of part 2 of the cuvette rotation

Part 2 begins at the maximum angle found in part 1,  $\theta_1 = \arctan \frac{2V}{ab^2}$ . To determine the terminal expression for  $\theta_2$  in this range, consider a right triangle of interior angle  $\theta_2$  and legs of length 'a' and ' $\frac{a}{\tan \theta_2}$ ' (see Fig. S5). As the volume of the solution is the product of the depth and area of the triangle, we determine the terminal angle as follows (analogous to part 1).

$$V = a\left(\frac{1}{2}\right)(a)\left(\frac{a}{\tan\theta_2}\right) \quad (10)$$

$$V = \frac{a^3}{2 \tan \theta_2} \quad (11)$$

$$\frac{2V}{a^3} = \frac{1}{\tan \theta_2} \quad (12)$$

$$\tan \theta_2 = \frac{a^3}{2V} \quad (13)$$

$$\theta_2 = \arctan\left(\frac{a^3}{2V}\right) \quad (14)$$

Thus in part 2, the cuvette rotates from  $\theta_1 = \arctan \frac{2V}{a}$  to  $\theta_2 = \arctan \frac{a^3}{2V}$ . Within this range of angles, we calculate the value of 'z' by solving a system of equations (see Fig. S6 and Eqn. 15).

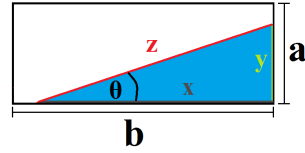


**Figure S6:** Cross-sectional view at an angle of rotation  $\theta$  in part 2.

$$\begin{cases} y = x \tan \theta \\ V = \frac{axy}{2} \Rightarrow x = \frac{2V}{ay} \end{cases} \quad (15)$$

We solve for 'y' by substituting the expression for 'x' into ' $y = x \tan \theta$ '.

$$y = \frac{2V}{ay} \tan \theta \quad (16)$$

$$y = \sqrt{\frac{2V}{a} \tan \theta} \quad (17)$$

Next, we substitute this value of 'y' back into ' $x = \frac{2V}{ay}$ ' to solve for 'x'.

$$x = \frac{2V}{a} \sqrt{\frac{a}{2V \tan \theta}} \quad (18)$$

$$x = \sqrt{\frac{2V}{a \tan \theta}} \quad (19)$$

Finally, using these values of 'x' and 'y' in the Pythagorean theorem, we solve for 'z'.

$$z = \sqrt{x^2 + y^2} \quad (20)$$

$$= \sqrt{\frac{2V}{a \tan \theta} + \frac{2V \tan \theta}{a}} \quad (21)$$

$$= \sqrt{\frac{2V \sec^2 \theta}{a \tan \theta}} \quad (22)$$

$$= \sqrt{\frac{2V}{a} \csc \theta \sec \theta} \quad (23)$$

Analogously to part 1, we represent SA as the following function of  $\theta$  in part 2:

$$SA_2(\theta) = az = a\sqrt{\frac{2V \csc \theta \sec \theta}{a}}, \quad \theta : \left[ \arctan \frac{2V}{ab^2}, \arctan \frac{a^3}{2V} \right) \quad (24)$$

### 3.1.3 Part 3

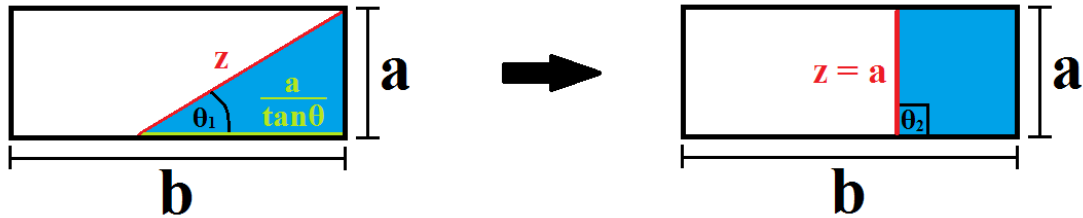


**Figure S7:** Definition of part 3 of the cuvette rotation

Part 3 begins at  $\theta_1 = \arctan \frac{a^3}{2V}$ . It ends at  $\theta_2 = \frac{\pi}{2}$  (vertical). To find the value of 'z', consider Fig. S8 as below.

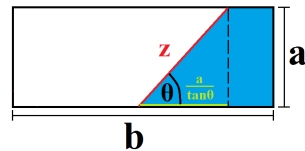


**Figure S8:** Cross-sectional view at an angle of rotation  $\theta$  in part 3.

We solve 'z' as follows:

$$z = \sqrt{a^2 + \frac{a^2}{\tan^2 \theta}} \quad (25)$$

$$= a\sqrt{1 + \frac{1}{\tan^2 \theta}} \quad (26)$$

$$= a\sqrt{1 + \cot^2 \theta} \quad (27)$$

$$= a\sqrt{\csc^2 \theta} \quad (28)$$

$$= a \csc \theta \quad (29)$$

Analogously to parts 1 and 2, we represent SA as the following function of  $\theta$  in part 3:

$$SA_3(\theta) = az = a^2 \csc \theta, \theta : \left[ \arctan \frac{a^3}{2V}, \frac{\pi}{2} \right) \quad (30)$$

Overall, the expression for the surface area of a fluid as it rotates in a square-bottom cuvette is:

$$SA(\theta) = \begin{cases} ab \sec \theta & : \theta \in \left[ 0, \arctan \frac{2V}{b^2 a} \right) \\ a\sqrt{\frac{2V \csc \theta \sec \theta}{a}} & : \theta \in \left[ \arctan \frac{2V}{b^2 a}, \arctan \frac{a^3}{2V} \right) \\ a^2 \csc \theta & : \theta \in \left[ \arctan \frac{a^3}{2V}, \frac{\pi}{2} \right) \end{cases}$$

## 3.2 Modeling

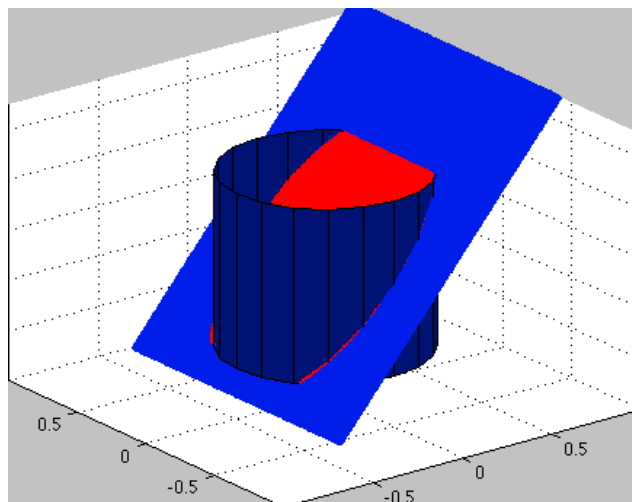


**Figure S9:** Computational model to measure area in arbitrary objects, where the points inside the vial are painted red, and points outside painted blue. The vial in this model is a perfect cylinder, although a polygon approximation is drawn.

To determine the relative surface area of fluids in non-rectangular vials as a function of rotation angle a simple computational model was developed. A plane of dense, equidistant point was rotated to the angle of interest, and superimposed onto the vial geometry. The number of points inside the vial were counted and the process repeated for each angle. In this scheme the axis of rotation is a function of the volume in the vial and for symmetrical, half-full vials the rotation axis is at the mid-height of the vial.

## 4 AFM analysis of nanosheet and monolayer heights

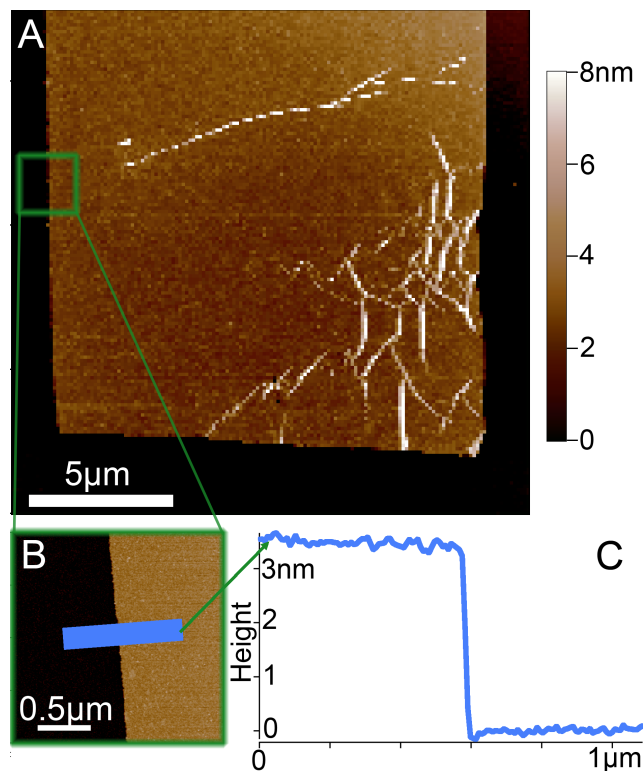


**Figure S10:** A: An AFM image of a nanosheet formed by rocking a vial of 10  $\mu\text{M}$  (Nae-Npe)<sub>18</sub> and (Nce-Npe)<sub>18</sub> in 10 mM AMPD buffer (pH 9), without NaCl, for 3 days with a 900s wait time between compressions. The buffer was removed from the sample by dialysis (Spectra/Por Float-A-Lyzer G2, MWCO 100 kDa). A 4  $\mu\text{L}$  drop of dialyzed sheet solution was deposited on freshly cleaved mica. The alternating contact (AC) mode AFM images were processed (1st order flattening and plane-fitting) in Igor Pro. B: Expanded image of red square shown in A. C: Profile average along the red square noted in B. We measure a  $3.4 \pm 0.4$  nm nanosheet thickness from the substrate.

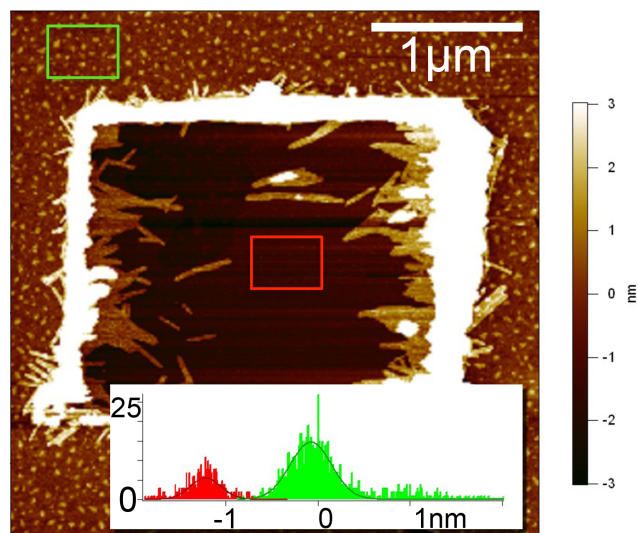


**Figure S11:** An AFM image of a  $(\text{Nae-Npe})_{18}$  and  $(\text{Nce-Npe})_{18}$  peptoid monolayer formed at a surface pressure of 42 mN/m, with a 10  $\mu\text{M}$  peptoid solution in 10 mM AMPD buffer (pH 9), 100 mM NaCl. The monolayer was transferred onto freshly cleaved mica by dipping the mica under a freshly aspirated surface and subsequently allowing a monolayer to form over the liquid surface over  $\approx 3$  minutes. The mica was then pulled vertically out at a rate of 1 mm/minute while maintaining the desired surface pressure with barrier control. A 2  $\mu\text{m} \times 2 \mu\text{m}$  region of the film was scraped away using high force contact mode imaging prior to the AC mode image shown above. The high force was not sufficient to discernibly scratch the underlying mica (not shown). The squares denote regions used to create the inset histograms. The monolayer thickness was determined to be  $1.2 \pm 0.3\text{nm}$ .

## 5 Powder X-ray diffraction analysis

**Table 2:** Comparison of X-ray diffraction spacings of peptoid nanosheets.

Assigned Peak	Shaken	Rotated
Sheet Stacking	27Å	28Å
Aromatic Interactions	5.3Å	5.4Å
Lateral Packing	4.5Å	4.6Å

X-ray diffraction data were collected at a multiple-wavelength anomalous diffraction and monochromatic macromolecular crystallography beamline, 8.3.1, at the Advanced Light Source located at Lawrence Berkeley National Laboratory. Beamline 8.3.1 has a 5 tesla single pole superbend source with an energy range of 5-17 keV. Data were collected with a 3x3 CCD array (ADSC Q315r) detector at a wavelength of 1.1159 Å. Data sets were collected with the detector 200 mm from the sample. Peptoid sheet solutions were in pH9 buffer, and the “rotated” sample also had 100 mM NaCl. The peptoid sheet solutions were concentrated approximately 100-fold in an Amicon Ultra centrifugal filter (100 kD MWCO, Millipore) then centrifuged at 13,200 rpm for 20 minutes. After removing the supernatant, the resulting peptoid sheet pellet was pipetted onto a Kapton mesh (MiTeGen). Data was processed with custom Matlab (Mathworks) scripts.

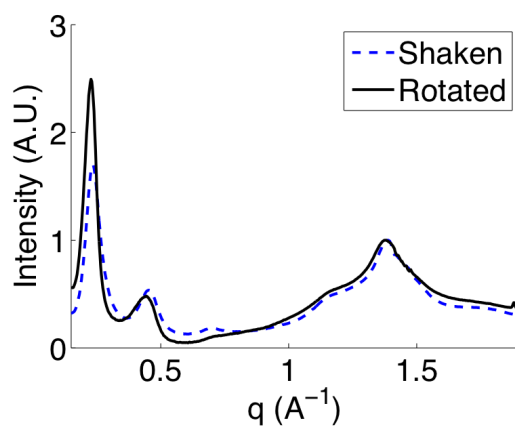


**Figure S12:** Radially averaged X-ray diffraction spectra, comparing nanosheets produced by vial shaking and vial rotating.

## 6 Sheet counting image analysis software

Quantitative sheet-counting was performed by sandwiching a known volume (e.g., 10  $\mu\text{L}$ ) of the 2  $\mu\text{M}$  Nile Red-stained nanosheet solution between a microscope slide and a coverslip of known area (e.g., 22x22mm). The slide was imaged at 5 random location under epifluorescence illumination with an Olympus IX81 inverted microscope fitted with an Andor iXonEM+ EMCCD camera.

Each image is analyzed in a custom Matlab (Mathworks) interface environment where human input guides the analysis (see Fig. S13). The human inputs consist of identifying a sample sheet, identify a representative background, setting the background threshold, minimum feature size and convexity-limit. All human inputs are recorded with the analysis output for reproducibility.

The user specifies the image scale, the volume of material and the area it was spread over. The user is then prompted to identify a sheet by clicking on it. Sheets are visually recognized by their uniform fluorescence and presence of apposed, straight edges along their long axis. The user is then prompted to click on the a region that does not contain sheets, as a background. The image is then intensity thresholded between the average value of the background and the average value of the sheet. The user can adjust this threshold to account for particularly noisy images. Features above the intensity threshold but below the minimum feature size are ignored. The remaining identified features are considered as either sheets or multi-layer aggregates, and are differentiated by their intensity. The user-specified aggregation parameter is the minimum multiplicative increase in intensity required to identify as a multi-layer, and is set to a default of 2 (i.e., more intense than a double-layer of sheets). The area of measured sheet material is divided by the volume of liquid in the image's field of view, as determined from the scale, the image size, and the volume per unit area. The resulting sheet area per unit volume is saved in a spreadsheet along with all of the the user-specified parameters.

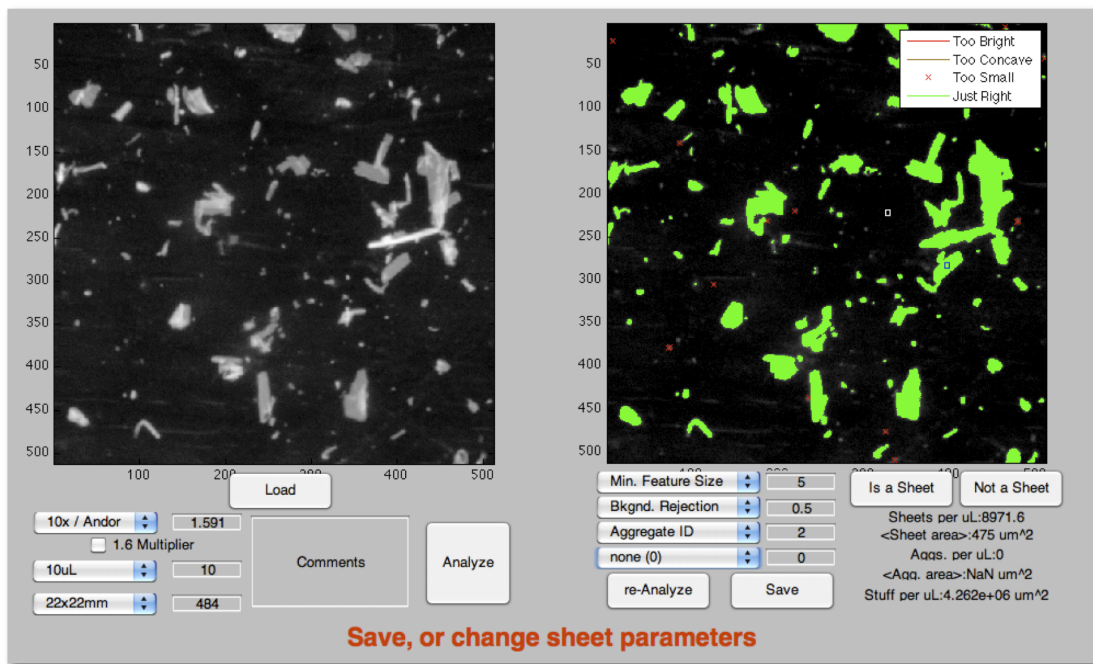


**Figure S13:** The user-interface for the Matlab-based sheet counting software.

## 7 Peptoid concentration effects

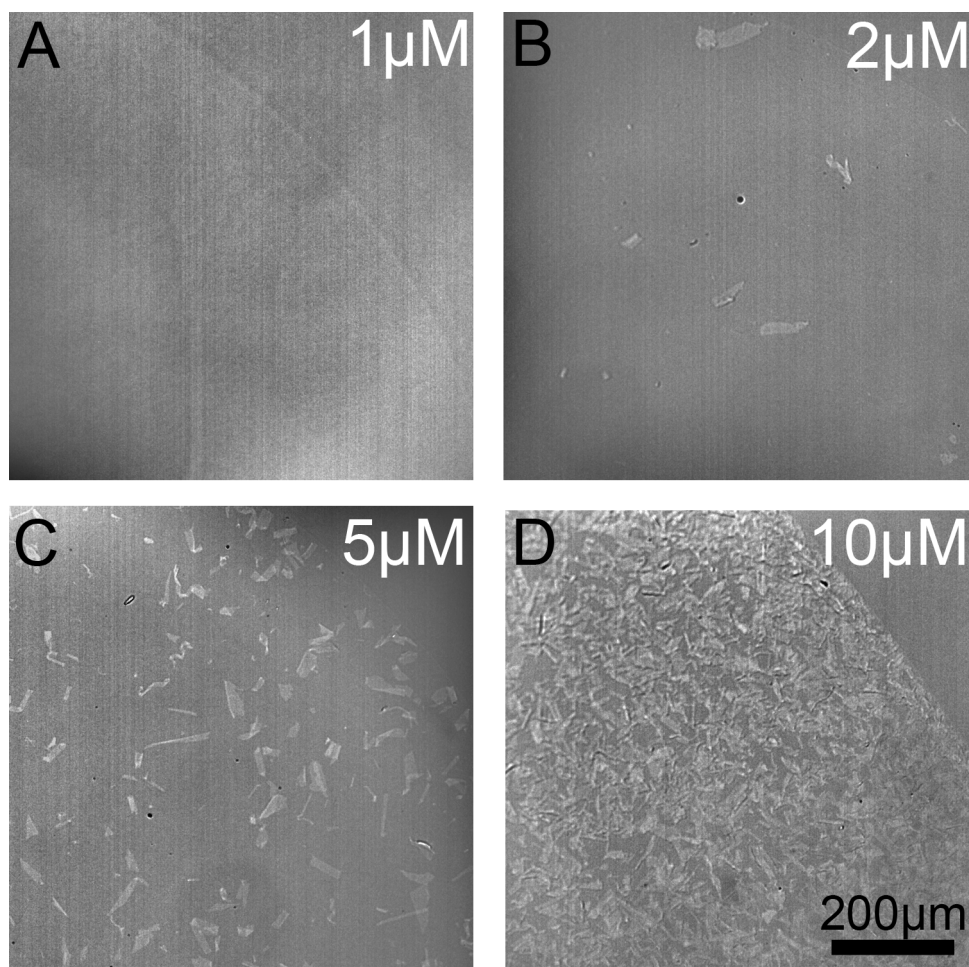


**Figure S14:** Differential Interference Contrast (DIC) images of peptoid nanosheets formed with different initial concentrations. The peptoid nanosheet solutions had been identically tumbled at 7RPM overnight in the standard vial, and  $1 \mu\text{L}$  subsequently deposited onto 1% agarose for imaging. The solutions were at 4 concentrations, as labeled, to qualitatively demonstrate that lower concentrations yield dramatically fewer sheets, at these production conditions. All the images were subsequently digitally treated with a high-pass filter at a  $100\mu\text{m}$  cut-off for clarity.

## 8 Zwittergent 3-12 inhibition of nanosheet production

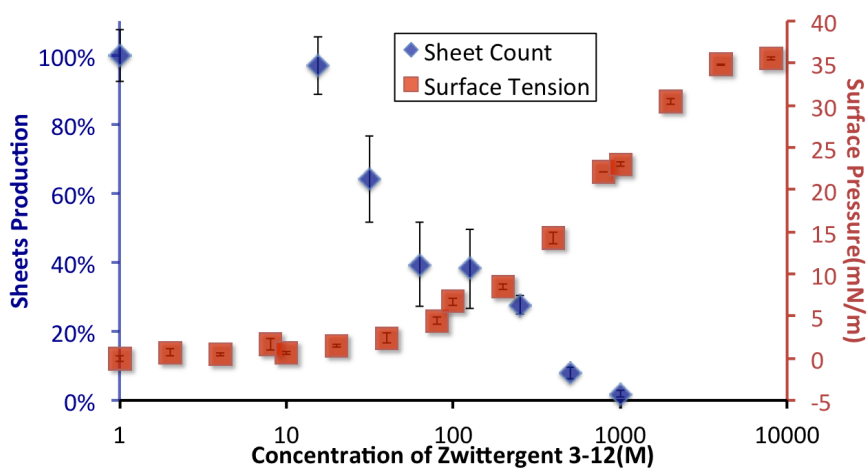


**Figure S15:** Peptoid nanosheet production and surface pressure as a function of the concentration of Zwittergent 3-12 (n-Dodecyl-N,N-dimethyl-3-ammonio-1-propanesulfonate) also present in solution. The 10  $\mu\text{M}$  (Nae-Npe)<sub>18</sub> and (Nce-Npe)<sub>18</sub>, 10 mM AMPD Buffer, 100 mM NaCl, pH 9 solution was rotated at 0.6 RPM for 20-26 hours. Sheet production was measured by software sheet counting, relative to a detergent-free sample. Surface pressure was measured by capillary rise. Error bars indicate one standard deviation.

## 9 Surface pressure reduction after multiple compressions

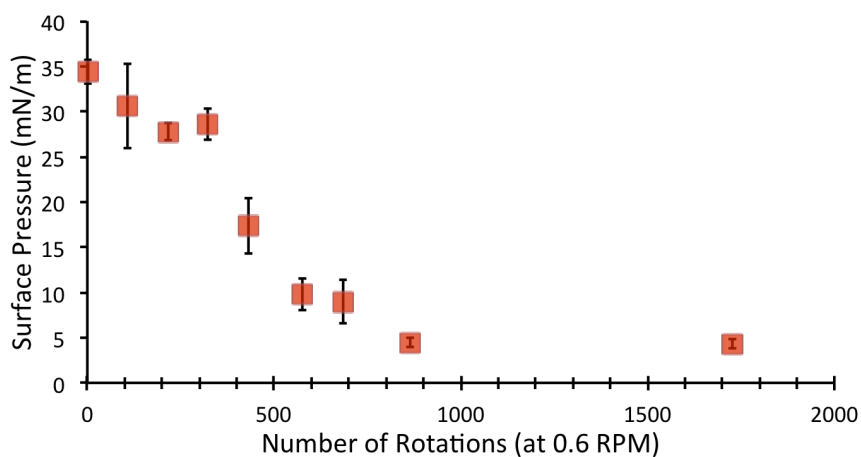


**Figure S16:** Surface pressure of 10  $\mu\text{M}$  (Nae-Npe)<sub>18</sub> and (Nce-Npe)<sub>18</sub>, 10 mM AMPD Buffer, 100 mM NaCl, pH 9 nanosheet forming peptoid solution as a function of the number of vial rotations, at 0.6 RPM. Surface pressure was measured by capillary rise on separate 3.5x1 cm cylindrical vials filled to 500  $\mu\text{L}$ . Error bars indicate one standard deviation of three sequential measurements.

## 10 Nanosheet formation by interfacial contact

The monolayer folding model implies that nanosheets are formed by contact between two apposed peptoid monolayers. This suggests that sheets could also be produced by direct interfacial contact of two monolayers, a phenomenon that is also likely to occur during vial shaking. We examined the viability of sheet formation by interfacial contact with a simple experiment and control. The experiment consisted of forcing interfacial contact by depositing subsequent droplets of nanosheet forming solution one on top of one another. The control consisted of a single, equivalent volume droplet of the same peptoid solution. The experiment and control were transferred onto an agarose gel and the presence of sheets was discerned by differential interference contrast optical microscopy (Leica DM4000).

We filled a 1 mL syringe with gently mixed 10  $\mu\text{M}$  (Nae-Npe)<sub>18</sub> and (Nce-Npe)<sub>18</sub> in pH 9 10 mM AMPD buffer 100 mM NaCl, and deposit a 20  $\mu\text{L}$  droplet onto a petri dish. We form a second 20  $\mu\text{L}$  droplet on the end of the needle and suspend it in air for a 30 s interval to allow monolayer expression at the air-water interfaces. Subsequently we deposited the droplet atop the first one to produce an interfacial contact. Controls without interfacial contact were prepared by deposition of a single 40  $\mu\text{L}$  droplet on a petri dish. We filter all the solutions immediately prior to drop depositions with 0.22  $\mu\text{m}$  PTFE membrane filter caps (Microsolv). To image the resulting sheets, the droplets are transferred to 1% agarose gel squares (preparation described above) with a 200  $\mu\text{L}$  micropipet and allowed to filter through the gel leaving macroscopic nanosheets on the surface. The presence of sheets is discernible by differential interference contrast optical microscopy (Leica DM4000) in air.

The analysis is complicated by the possibility of inadvertently generated nanosheets. For example, inadvertent sheets could be produced as the droplets are transferred onto agarose by micropipetting (e.g., by expansion and compression of the air-water interface while filling and emptying a conical shaped pipette tip), or by fluid dynamics that disturb the interface during deposition of the droplets. Therefore we limit our discussion to qualitative differences of the drop-on-drop experiments vs. the single-drop controls.

Samples that experienced interfacial contact exhibited significantly more, and larger, nanosheets than the single-drop controls (see Fig. S17 for representative images). The overall quantity of sheets remains small with respect to other sheet preparation techniques (e.g., shaking or tumbling, see Fig. S1).

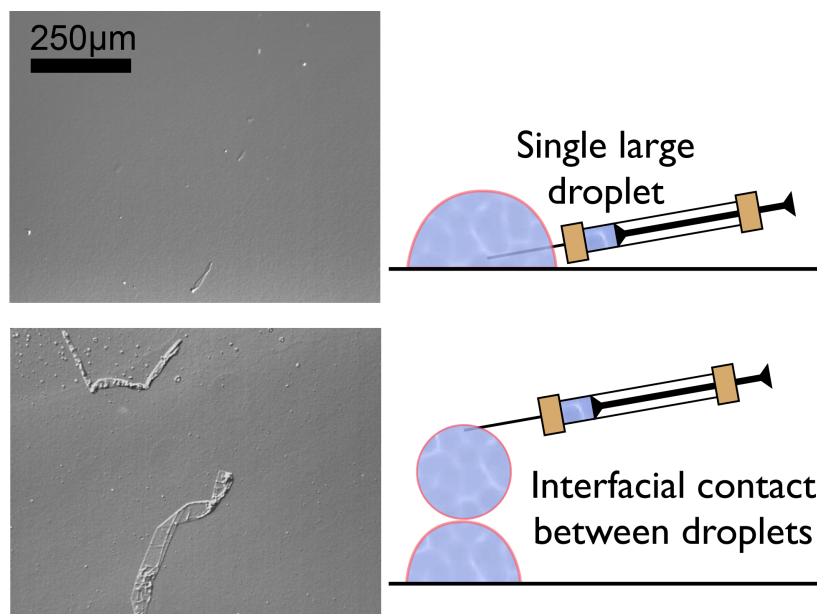


**Figure S17:** Optical differential interference contrast images of peptoid solutions filtered through agarose gel to reveal macroscopic nanosheets. Images were high-pass filtered to correct for uneven illumination, and the scale bar is consistent across the images. Top: Nanosheets filtered from a single  $40\mu\text{L}$  droplet (see right). Bottom: Nanosheets filtered from two  $20\mu\text{L}$  droplets that were brought into interfacial contact.

## 11 Peptoid synthesis

Peptoid oligomers were synthesized on an automated robotic synthesizer using the solid-phase submonomer method. In this method, the Fmoc group on Rink amide resin (0.61 mmol/g, Novabiochem, San Diego, CA) was deprotected with 20% 4-methylpiperidine in DMF (v/v) before starting the submonomer cycle. Peptoid synthesis on resin was carried out as follows: a 0.6 M solution of bromoacetic acid in DMF (1.13 mL, 1.35 mmol) and 0.93 eq. of N,N-diisopropylcarbodiimide (0.20 mL, 1.25 mmol) was added to a resin-bound amine (50  $\mu$ mol) and mixed for 20 min at 35C during acylation step of the submonomer cycle. After washing, the resin-bound bromide was then displaced with the amine submonomer by adding a 2 M solution of the amine in N-methylpyrrolidinone. The displacement reaction was carried out for 60 or 120 minutes at 35C for residues 1-18 or 19-36, respectively. The crude peptoid products were cleaved from the resin with 95:5 trifluoroacetic acid (TFA):water (v/v) for two hours at room temperature.

The cleavage solution was filtered and evaporated under a stream of nitrogen gas to remove the TFA. The crude peptoid product was then dissolved in a 1:1 mixture (v/v) of water/acetonitrile and subjected to further purification through reverse-phase HPLC on a Vydac C18 column (10  $\mu$ m, 22 mm x 250 mm), using a gradient of 30-60% acetonitrile in water with 0.1% TFA over 60 min. All final products were analyzed by analytical reverse-phase HPLC (30-55% or 40-80% gradient at 1 mL/min over 30 minutes at 60 C with a C18, 5  $\mu$ m, 2 x 50 mm column) and matrix- assisted laser desorption/ionization mass spectrometry (MALDI, Applied Biosystem/MDS SCIEX 4800 MALDI TOF/TOF Analyzer). The final peptoid products were lyophilized, dissolved in 100 mM HCl (aq) and then lyophilized again. This step was repeated two more times to ensure formation of the hydrochloride salt.

## 12 Solvatochromic dye conjugate structure

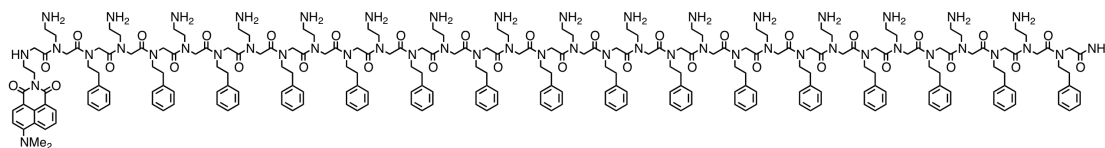


**Figure S18:** Structure of solvatochromic fluorophore 4-N,N-dimethylamino-1,8-naphthalimide dye conjugate incorporated into the peptoid backbone. Mass and purity were determined using MALDI and HPLC protocols described above. Observed mass of 4521.59 (4521.49 predicted), 94% purity. The solvatochromic dye monomer, 2-(2-Aminoethyl)-6-(N,N-dimethylamino)-1H-benzo[de]-isoquinoline-1,3(2H)-dione, was synthesized according to literature procedures[2].

### 13 The vial rocking device

The vial rocking device consists of a BASIC programmable micro-controller (Basic Stamp 2pe Parallax Inc., Rocklin, CA), a gear motor (#155821, Jameco, Belmont, CA), an optical rotary encoder, a pulse width modulation counter module to control motor speed (PWMPAL, Parallax Inc., Rocklin, CA), and a reed switch used for homing the position between cycles. A belt from the gear motor rotates a platform that holds the vials, whose shaft is connected to the optical rotary encoder. A video of a full cycle of the vial rocking device is included (rocking\_device\_cycle.mov).

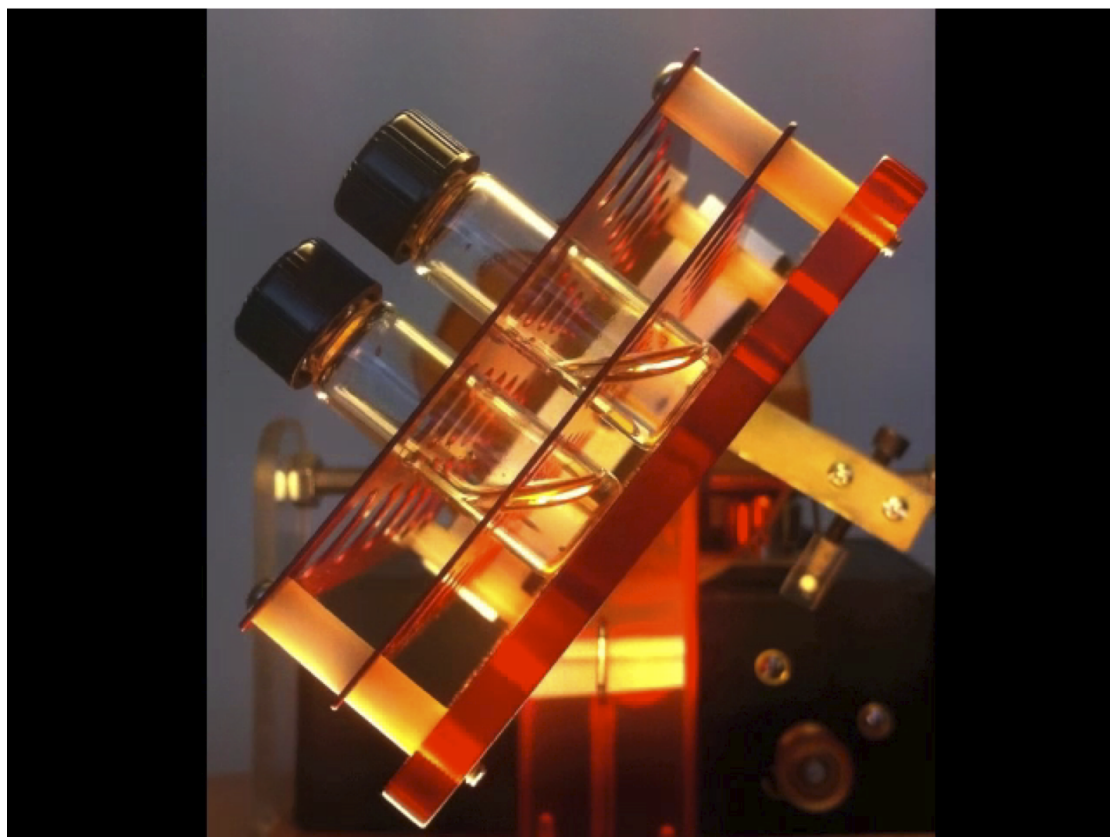


**Figure S19:** End-on view of the vial rocking device during a rotation. The device rotates up to 20 vials in parallel.

## References

- [1] Maaloum, M., Pernodet, N. and Tinland, B. Agarose gel structure using atomic force microscopy: gel concentration and ionic strength effects. **19** 1606-1610, *Electrophoresis*, 1998.
- [2] Wu, A.; Xu, Y.; Qian, X. Novel naphthalimideindomethacin hybrids as potential antitumor agents: effects of linkers on hypoxic/oxic cytotoxicity and apoptosis-inducing activity **143** 893-899. *Monatshefte für Chemie*, 2010.